Pressure and contact area in the coxofemoral joint during activities from finite element parametric modelling

Sébastien THIBAUD[a], Mylène VILLARS[b], Fabrice RICHARD[b*]

[a)] Université Marie et Louis Pasteur, SUPMICROTECH, CNRS, institut FEMTO-ST, F-25000 Besançon, France

[b*)] Université Marie et Louis Pasteur, CNRS, institut FEMTO-ST, F-25000 Besançon, France

*fabrice.richard@univ-fcomte.fr

Abstract

The determination of pressure and contact area distributions in the coxofemoral joint during activities of daily living is essential to predict joint degeneration and prosthesis wear. This can also provide biomechanical justifications for preoperative planning and postoperative rehabilitation. To study the temporal evolution of pressure fields and contact areas in a person's coxofemoral joint during different activities, a parametric finite element model of the joint is developed. Eight activities of daily living are studied. Two different laws of cartilage behaviour are used: elastic and hyperelastic. The results obtained focused on a single subject are compared with those of other studies using classical hypotheses: no labrum, synovial fluid and bone deformability neglected, ideal spherical geometry of the articular surfaces and frictionless contact. The results show that activities related to sitting in and getting up from a chair are the least burdensome activities for the hip joint. Alternation between the bipodal station and the monopodal station is the most restrictive activity. For most activities, the highest pressures are in the anterolateral upper region of the femoral head and in the antero-superior region of the cotyloid. For the activities studied, considering the hyperelasticity of cartilage does not generate a significant difference compared to a simple elastic behaviour. The results are globally in agreement with numerical and analytical models using a spherical model of the joint and quantitatively enrich the knowledge of this field.

1. Introduction

Mechanical factors play an essential role in the development and progression of osteoarthritis. The cartilage can withstand extremely high loads, but when the morphology of the joint is abnormal (i.e., during dysplasia, which results in a femoral-acetabular conflict) or during a biochemical alteration of the structure of the cartilage, the latter is no longer able to withstand such loads and gradually deteriorates. According to some authors, osteoarthritis is due to high local pressures [1–3]. Knowledge of pressure fields and contact areas in the joint would allow a better understanding of non-pathological and pathological mechanical behaviour of the hip and the effects on cartilage. Despite some recent developments [4], musculoskeletal models [5] developed lack methods for estimating cartilage contact pressures but some computational approach provide the means to predict pressure fields and contact areas: the discrete element analysis [1,3] and the finite element method [6–9]. These studies reported proof-of-concept and results of parametric studies but simplifying assumptions and a lack of validation limited their ability to provide definitive measurements of the magnitude and distribution of pressure field and contact area in normal hips during activities of daily living.

Geoffrey Ng [10] investigated the effects of cam femoroacetabular impingement on hip joint loading through finite element analysis, incorporating subject-specific geometries obtained from CT scans during quasi-static positions ranging from standing to squatting. In this instance, the findings reveal a concentration of maximum shear stresses in the anterosuperior region of the underlying bone during squatting. The kinematics of the squat motions were recorder using motion capture cameras and the kinetics were

recorded using fixed force plates. Akrami et al. [11] propose a finite element approach to investigate the behaviour of the hip joint by generating the model from CT scan images. The forces generated by the ligaments are applied using spring elements, where the equivalent stiffness values are defined to represent the overall stiffness of each ligament. A sole loading scenario is considered, specifically the one-legged stance, and is approximated by applying a static force perpendicular to the acetabulum at the extremity of the femur length. This case is highly restricted, yet it serves to demonstrate the feasibility of obtaining a simulation model from medical imaging data of actual patients. Clarke et al. [12] also employed a finite element model derived from CT images. Through a design of experiments with a full factorial approach, they investigate the impact of various parameters (material stiffness distribution, loads imposed by muscles, location of boundary conditions, hip joint contact conditions), incorporating geometry variability across eight patients. They considered two static load cases; these were the maximum joint reaction forces experienced during normal walking and moving from sitting to standing from the study of Bergmann et al. [13]. A sensitivity analysis is then performed in the case of the maximum joint reaction forces cases. Kinematics and time dependant loading are not considered, but this demonstrates the feasibility of conducting sensitivity analysis on representative, static, complex models derived from real patients.

To determine evolution of forces in the hip joint several approaches are used. In the first instance, the use of a recording system employing cameras to capture movements and force plates to assess the changes in forces was implemented as used by Geoffrey Ng et al. [10]. But it needs an inverse dynamic approach to obtain forces in the hip joint. A second way is to use musculoskeletal modelling, but it needs some optimization techniques to calculate muscle forces, which influence resultant hip contact forces [14,15]. Another way,

is to use instrumented prostheses to directly determine the forces involved in the hip joint as proposed by Bergmann et al. [13].

Given that the study for Bergmann et al. [13] is widely considered as the benchmark for determining the changes in forces and movement in the hip joint, these variations are used in the present work as input data (joint rotations and applied forces) during the activities. To estimate the pressure field at the contact surfaces of the joint and the values of the pressure peaks, a finite element Hip Joint Parametric Model (HJPM) is proposed. Eight activities of daily living are studied in the context of a spherical pattern of the joint and an elastic behaviour of the cartilage. As some studies model cartilage using hyperelastic behaviour [9,16], the influence of considering hyperelasticity.

The main interest of having the mechanical fields at the contact level for the activities studied is to better understand the appearance of osteoarthritis in a healthy joint or its aggravation in people with beginner coxarthrosis or a congenital deformity, e.g., dysplasia. Another interest of the study is the parametric model developed (HJPM) developed to achieve the results. HJPM can be useful in orthopaedic and traumatological surgery to carry out a preoperative osteotomy schedule and in rehabilitation to define a postoperative schedule. HJPM can also help address an industrial need to optimize the geometry and surface properties of hip replacements. The surfaces of the intermediate hip prostheses are in direct contact with the cartilage of the natural cotyloid. Knowledge of the mechanical fields in this contact is therefore essential to design prosthesis surfaces more suitable for the cartilaginous surfaces of the cotyloid and thus preserve them from wear.

2. Materials and methods

To study the mechanical behaviour of the coxofemoral joint during different activities, a model based on Hip Joint Parametric Model (HJPM) was developed. For a given activity and a particular subject, HJPM makes it possible to simulate the temporal evolution of pressure fields and contact areas in the coxofemoral joint. For these simulations, the experimental data (kinematics of the articulation and evolution of the load) of Bergmann et al. [13] of the KWR subject are used (Table 1). Eight activities are studied: walking (slow, normal, quick), going downstairs, going upstairs, standing up, sitting down, monopodal support and bipodal support alternation.

Table 1: Characteristics of the KWR subject [13]

Patient	**KWR**
sex	male
age	61 years
height	165 cm
weight	702 N
implanted side	right

HJPM is developed in Matlab script. For a given activity and the subject studied, HJPM generates a script that can be interpreted by the finite element software Ansys Mechanical APDL. Once the simulation of the activity has been carried out, the finite element results are processed using Matlab scripts to quantify the temporal evolution of the pressure fields and contact areas. HJPM then makes it possible to automatically generate the loading conditions in parametric form, to carry out the associated simulations and to extract the desired mechanical.

2.1. Geometry and meshing

Three possible geometric shapes of articulation are programmed in HJPM: spherical, ellipsoidal and conchoidal. For the spherical pattern of the joint used in this study, the circular profile is defined by an angle α_p and an external radius R_0 in the plane (X_{loc}, Y_{loc}) (Figure 1).

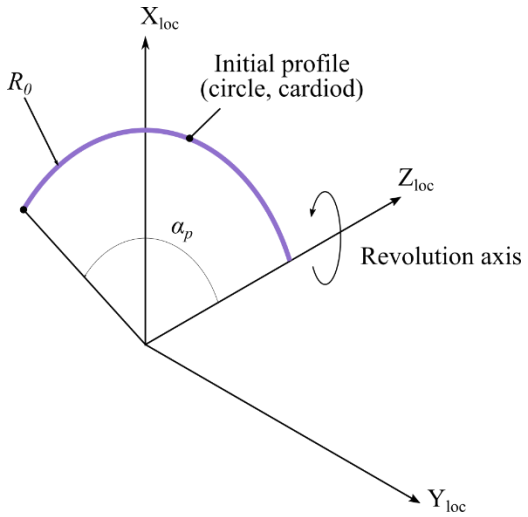

Figure 1: Initial profile and associated coordinate system ($\alpha_p = 150°$, $R_0 = 24$ mm).

The inner surface of the femoral head is constructed by rotating the profile along the Z_{loc} axis. The quadrangular mesh thus obtained is defined by a number of elements in the profile (n_{Profil}) and around the axis of revolution (n_{Revol}). Using extrusion of this mesh according to the normal to the surface, we obtain the final density mesh with n_{E_p} hexahedral elements in the thickness E_p of the femoral cartilage (Figure 2a). According to Athanasiou et al. [17], $E_p = 2.66$ mm.

The cotyloid cartilage is built according to the same principle except for the revolution of the profile, which is incomplete to model the acetabular fossa (Figure 2b). To do this, three angular parameters are needed: θ_0, θ_f and θ_c with:

$$\tan \theta_0 = \frac{w}{R} \tag{1}$$

where R and w are the inner radius of the cotyloid and the width of the acetabular fossa, respectively .

No inter-articular space is considered here. According to Naish et al. [18], magnetic resonance imaging shows no influence of this parameter. A representation of the meshes is given in Figure 2. The mesh consists of using of 8-nodes fully integrated hexahedral elements (9380 elements). It leads to consider four integration points in thickness. It is based on a mesh convergence analysis with a strain energy error less than 2% between 3 and 2 elements in thickness.

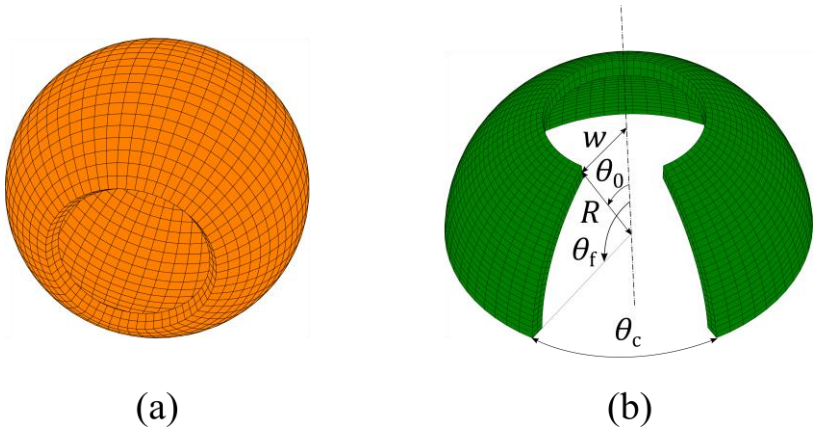

Figure 2: Meshing and parameterization of cartilage: a) femoral b) cotyloid.
($R = 24$ mm, $w = 12$ mm, $\theta_f = 90°, \theta_c = 60°, n_{Profil} = 35, n_{Revol} = 70, n_{E_p} = 2$)

2.2. Cartilage behaviour

The activities studied are fast enough to neglect the viscous and/or poroelastic effects on cartilage behaviour [19]. However, the activities studied are slow enough to neglect the inertial effects. Two isotropic behaviours are tested to study a possible difference in the results: linear elastic (Hooke) and hyperelastic (Mooney-Rivlin). The elastic behaviour is defined by its elastic strain energy density W_E, which is a quadratic function of the infinitesimal strain tensor $\boldsymbol{\varepsilon}$:

$$W_E(\boldsymbol{\varepsilon}) = \frac{1}{2} C_{ijkl} \varepsilon_{ij} \varepsilon_{kl} \tag{2}$$

Where C_{ijkl} is the fourth order elastic tensor depending on the Young's modulus E and the Poisson's ratio ν. The hyperelastic material is defined by its elastic strain energy density W_H, which is a function of the elastic strain state. The Mooney-Rivlin strain energy density function is expressed as:

$$W_H(\bar{I}_1,\bar{I}_2,J) = C_{10}(\bar{I}_1 - 3) + C_{01}(\bar{I}_2 - 3) + \frac{1}{D_1}(J-1)^2 \quad (3)$$

Where $\bar{I}_1, \bar{I}_2$ are the first and second invariant of the isochoric-elastic right Cauchy-Green deformation tensor and J the elastic volume ratio. C_{10}, C_{01} and D_1 are the three material parameters.

Both of these behaviours are frequently used in this type of study [1,6,9,20,21]. To ensure that the elastic and hyperelastic models equivalent in small deformation assumptions, Young's modulus ($E = 8$ MPa) and Poisson's ratio ($\nu = 0.49$) are obtained from hyperelastic parameters (C_{10} =1.31 MPa, $C_{01} = 0.03$ MPa, $D_1 = 0.015$ MPa^{-1}) using the two following relations:

$$4(C_{10} + C_{01}) = \frac{E}{1+\nu} \quad (4)$$

$$D_1 = \frac{6(1-2\nu)}{E} \quad (5)$$

The parameter values are consistent with those identified by Richard et al. [22] for healthy cartilage.

2.3. Resolution and post-processing

The cotyloid and femur are positioned relative to the pelvis at each moment of movement (Figure 3.a) in accordance with the kinematic data and images of Bergmann et al. [13].

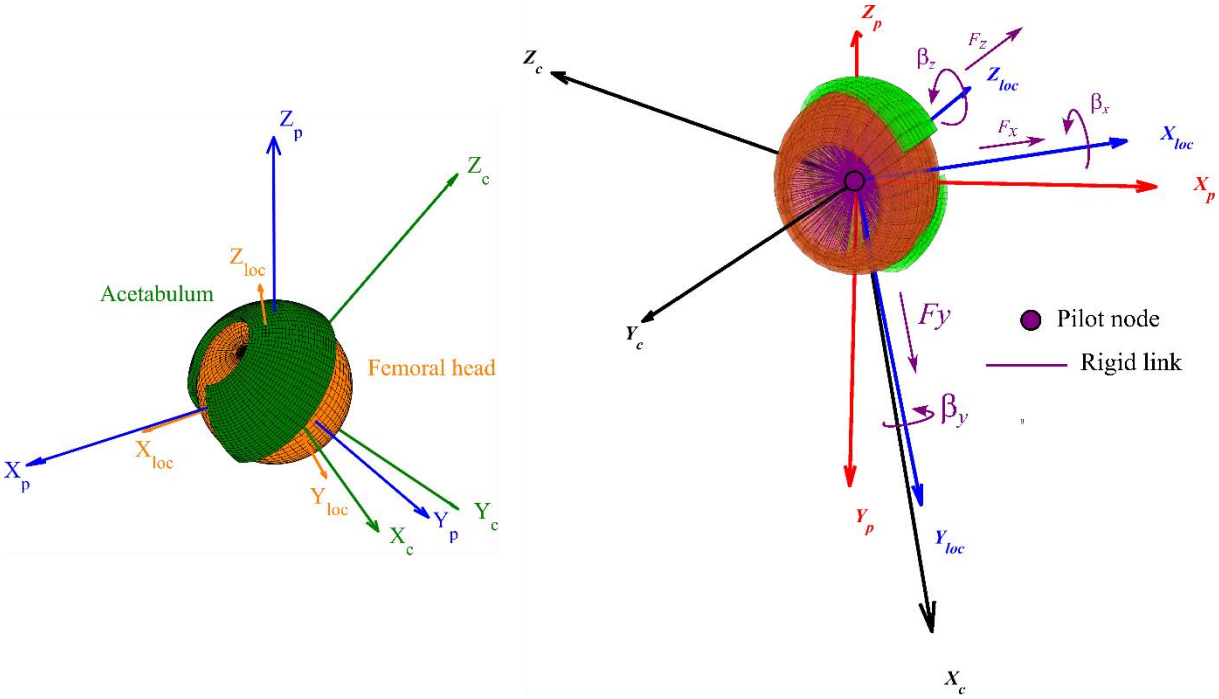

a. b.

Figure 3: (a) Mesh size and coordinate systems: *p* (pelvis), *c* (cotyloid), *Loc* (femur), (b) Applied loading and boundary conditions.

For a given geometric configuration and loading, a quasi-static simulation using the finite element software leads to stress, strain, and displacement fields in the cartilage. To achieve this, a pilot node is established at the centroid of the hip joint, where the sensors are positioned (Figure 3.b). Rigid links are then specified to connect the pilot node to nodes located on the interior face of the femoral head. From the results of Bergman et al. [13], the experimental forces $\left(F_x(t), F_y(t), F_z(t)\right)$ obtained from instrumented prosthesis are applied to the pilot node. Simultaneously, based on the biomechanical study, angular positions $\left(\beta_x(t), \beta_y(t), \beta_z(t)\right)$ of the femoral head are enforced (see Figure 4.a and Figure 4.c for example in the case of Walking Normally). The model considers time-dependent paths and time-dependent loading cases to determine the evolution of contact pressure and stress distribution during various loading conditions, both spatially and temporally. The contact between the two cartilages is assumed to be frictionless and is controlled by

an augmented Lagrangian type algorithm. The acetabulum is considered as fixed in the local configuration.

HJPM allows discretizing the cycle of the movement in identical time steps to perform the simulation of a complete movement using an automatic loop by updating the geometric configuration and the associated loading at each time step depending on the experimental discretization. To analyse the contact pressures $p(x, y, z)$ and contact areas A during the activities, several variables are computed at each time t:

- Maximum pressure $p_{max}(t)$, mean pressure $p_{mean}(t)$ as well as minimum pressure $p_{min}(t)$ and contact areas $A(t)$. The contact area surface between the femoral head and the cotyloid is calculated from the elements for which the pressures at the nodes are nonzero.
- The contact pressure field on the femoral surface at the time of pressure peaks using a stereographic projection [23] facilitates the location of pressure points. This method consists of projecting a sphere onto a plane. The nodes of the upper part of the femoral head are projected on the transverse plane containing the centre of the femoral head and normal to the vector joining this centre and the upper pole of the femoral head. In this way, the pressures calculated at each node are projected (see Figure 5).

3. Results

First, the results obtained from the proposed approach are detailed for a normal walk. A complete summary of the results for eight activities is then presented and discussed: walking slowly (WS), walking normally (WN), walking quickly (WQ), going downstairs (GD), going upstairs (GU), standing up (SU), sitting down (SD), monopodal support and bipodal support alternation (BMA).

3.1. Detailed results for walking normally

The walking cycle is carried out at a speed of 1.09 m/s and can be broken down into several phases. Nine positions are thus identified in Figure 4 to present the evolution of the load (force), the kinematics of the joint (3 rotations) and the results of the simulation of the movement in terms of pressures and contact areas.

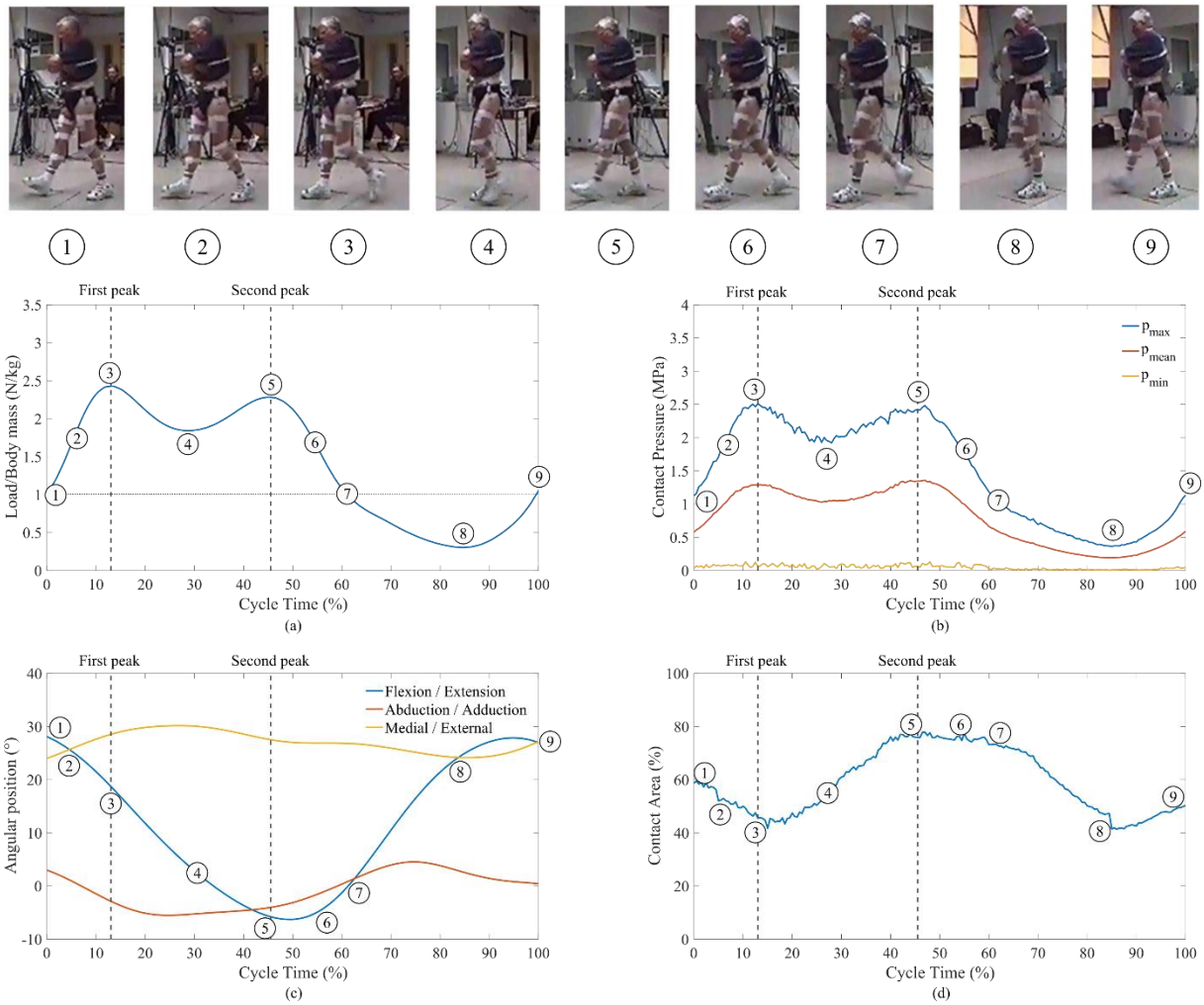

Figure 4: Temporal evolution of (a) imposed load, (c) imposed angles,
(b) calculated contact pressure, (d) calculated relative contact areas.
Case of walking normal (WN) [13]: 1- contact of the heel on the ground; 2- middle of the doubling anterior reception support phase; 3- beginning of the monopodal support phase; 4- middle of the monopodal support phase ; 5- end of the monopodal phase; 6- pre-oscillation phase; 7- beginning of the oscillation phase; 8- middle of the oscillation phase; 9- end of the oscillation phase.

Table 2 summarizes the values of the pressures (maximum and average) and the contact areas at the nine positions.

Table 2: Pressures and contact area for the nine normal walking (WN) positions.

Position	Cycle time	Contact pressures		Contact area
No.	%	p_{max} (MPa)	p_{mean} (MPa)	A (% of the total area)
1	0.0	1.12	0.58	58.62
2	4.5	1.65	0.88	56.20
3	13.0	2.51	1.29	45.63
4	29.5	2.00	1.05	60.16
5	45.5	2.42	1.35	75.95
6	55.5	1.70	0.96	75.37
7	61.5	1.06	0.60	73.33
8	85.0	0.36	0.19	41.44
9	100	1.13	0.59	50.28

Figure 5 shows the contact pressure field on the cartilage of the femoral head for the nine studied positions.

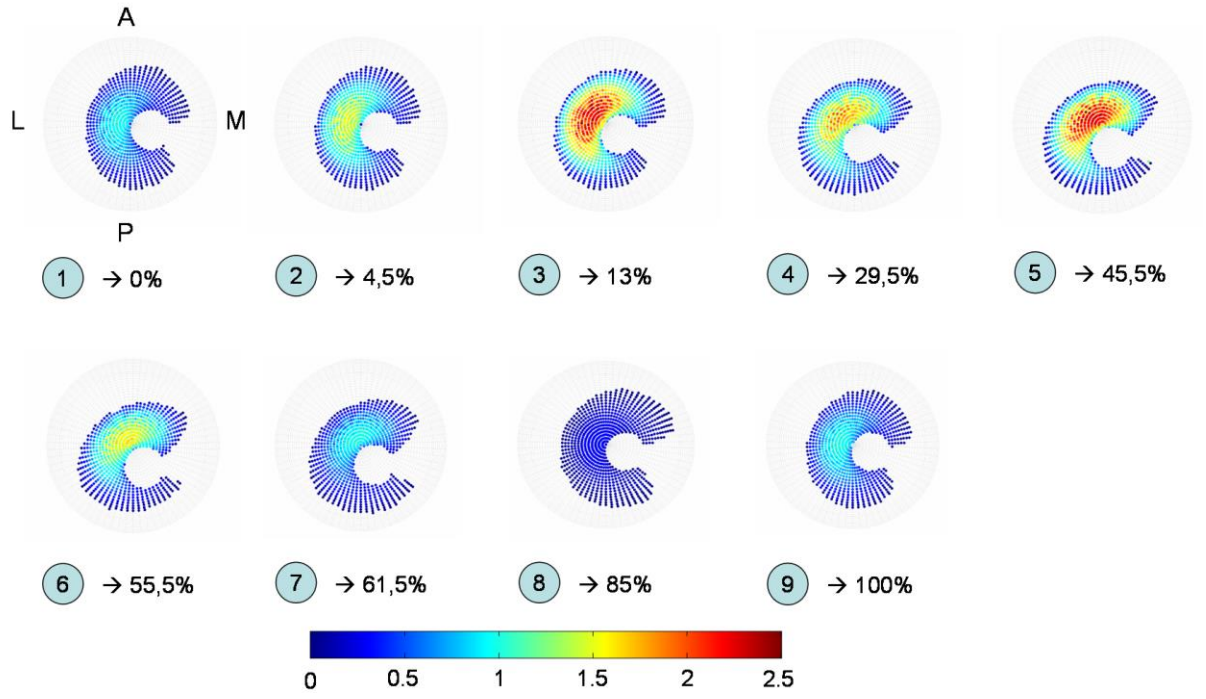

Figure 5: Normal walking activity (NW). Projection of the contact pressure field (in MPa) on the cartilaginous surface of the femoral head as a function of the % of the cycle time.
(A: previous; P: posterior; L: lateral; M: medial).

3.2. Summary results for eight activities

The application of the method for all activities as presented previously for one case (WN) is then applied to the other activities. Results are summarized in terms of contact pressures, contact area and of average values over a cycle of movement.

For the eight activities, the temporal evolutions of the contact pressures on the articular surfaces mimics the applied force. The values of the pressure peaks, contact area and cycle time are reported in Table 3. Table 4 summarizes the location of the contact pressure peaks for the different movements studied.

Table 3: Summary of pressures and contact areas at the time of peak pressures for different activities.

Activity	Contact pressure		Contact area	Cycle time
	p_{max} (MPa)	p_{mean} (MPa)	A% (% of total area)	%
1st pressure peak				
WS	2.51	1.28	37.6	19.0
WN	2.51	1.29	45.6	13.0
WQ	2.90	1.47	52.0	12.5
GU	3.16	1.45	61.9	15.5
GD	3.37	1.73	73.9	54.5
SU	2.28	1.20	80.9	39.5
SD	**1.96**	1.03	79.1	49.0
BMA	**3.98**	2.08	80. 6	67.0
2nd pressure peak				
WS	2.66	1.33	69.9	43.5
WN	2.48	1.36	77.9	47.0
WQ	2.57	1.38	75.7	45.5
GU	2.90	1.49	71.7	47.5
GD	3.39	1.83	84.0	90.0

Table 4: Localization of the contact pressure peaks for the eight movements.

Activity	Localization	
	1st pressure peak	
	Femoral head	Cotyloid
WS	Superior latero-anterior	Superior
WN	Upper antero-lateral	Antero-superior
WQ	Lateral-anterior superior	Superior
GU	Upper antero-lateral	Superior
GD	Upper antero-lateral	Superior-anterior
SU	Upper mid-posterior	Postero-superior
SD	Superior-posterior	Postero-superior
BMA	Upper antero-lateral	Superior-anterior
	2nd pressure peak	
WS	Upper antero-lateral	Antero-superior
WN	Upper antero-lateral	Antero-superior
WQ	Upper antero-lateral	Antero-superior

GU	Upper antero-lateral	Antero-superior
GD	Superior-lateral	Antero-superior

Figure 6 shows in the form of histograms the averages and standard deviations over a cycle of the pressures (maximum $\bar{p}_{max}$ and mean $\bar{p}_{mean}$) and the contact areas $\bar{A}$ for the eight activities.

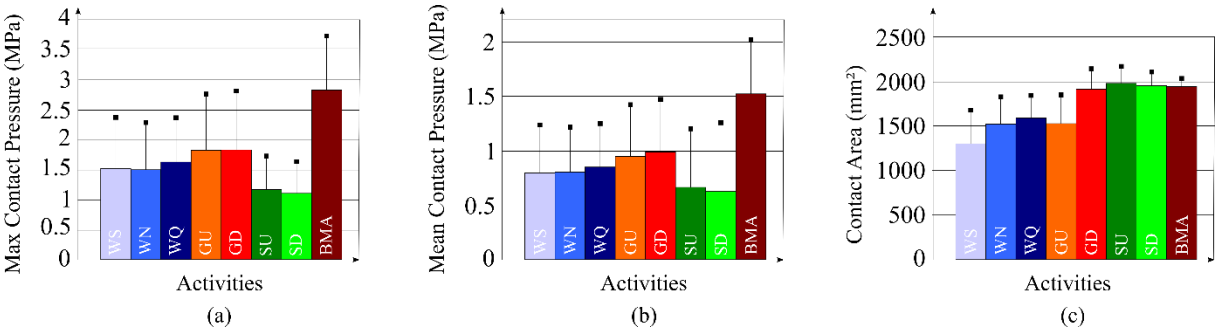

Figure 6 Comparison of the averages and standard deviations over a cycle of the (a) maximum pressures $\bar{p}_{max}$, (b) mean pressures $\bar{p}_{mean}$ and (c) contact areas $\bar{A}$ for the eight activities (the bars represent the standard deviations).

Given the high values of the standard deviations, an analysis of variance is conducted to identify the significant differences between the eight activities. In the case where the analysis of variance is significant, a post hoc test is also performed with a significance level of 5%.

Four activities (WQ, SU, GU and BMA) are also tested assuming the behaviour of near-incompressible hyperelastic cartilage. The differences in the results between the two hypotheses (elastic and hyperelastic) are negligible (<1%).

4. Discussion

In terms of peak values and location, the results for all activities are in agreement with the results of Bachtar et al. [6] and Pawaskar et al. [24]. It leads to the following analysis:

- The highest maximum pressure peak is observed during the alternation between the bipodal station and the monopodal station with $p_{max}(67\%) = 3.98$ MPa.
- The lowest maximum pressure peak is obtained for the activity "sitting on a chair" with $p_{max}(49\%) = 1.96$ MPa. This result is consistent with that of Pawaskar et al. [24]. In contrast, Yoshida et al. [1] obtained the highest maximum pressure peak value for this movement. The value calculated by Pawaskar et al. using the finite element method is 2.57 MPa, while that calculated by Yoshida et al. using the discrete element method is 9.36 MPa. This surprisingly high value obtained by Yoshida et al. is explained by the contact area at the time of the peak, equal to only 19.7% of the total area and located at the outer edge of the cotyloid. This high value is therefore probably due to an edge effect. The contact area obtained by Pawaskar et al. at the time of the peak is 49.9%. This value is higher than that found by Yoshida et al. (19.7%) and lower than the one we obtain (79.1%). This difference can be explained by the geometry of the acetabulum considered by Pawaskar et al. as not spherical.
- The pressure peaks during staircase descent are higher than those during staircase climbing.
- For the activities of rising and sitting, the peak of maximum pressure is obtained when the hip has almost reached its maximum flexion.
- For walking (WS, WN, WQ), climbing and descending stairs, the first pressure peak occurs at the beginning of the monopodal phase, and the second peak occurs at the end of the monopodal phase. These results are consistent with several studies [1,24,25]. For these 5 activities, the contact areas are higher at the time of the 2nd pressure peak, which corresponds to the maximum extension of the hip.

The peak locations change depending on the activity and during movement. For most activities, the highest pressures are in the anterolateral upper region of the femoral head

and in the antero-superior region of the cotyloid. The findings from Harris et al. [26] align with our own results. Their study also revealed that the highest pressures are concentrated in the anterior and superior regions of the acetabulum during walking and stair descent activities. Some authors [1,27] have hypothesized that the distribution of cartilage thickness is related to mechanical stresses, and indeed, the regions of higher pressures correspond to those of higher thicknesses [28,29,18,30]. In the presence of osteoarthritis, the thickness of the cartilage decreases where it is most stressed. Our results are consistent with clinical observations because cartilage degeneration occurs in the upper part of the hip joint [31].

According to Figure 6 and analysis of variance, the pressures $\bar{p}_{max}$ and $\bar{p}_{mean}$ are:

- significantly different between walking and the other activities,
- significantly higher between alternating between bipodal and monopodal (BMA) stations and all other movements. The BMA movement is therefore the most restrictive for the hip joint.
- not significantly different between getting up and sitting down, which are the two least constraining movements for the hip joint,
- not significantly different between the different walking speeds,

According to Figure 6 and analysis of variance, the average area $\bar{A}$ is:

- significantly lower for slow walking than for all other movements,
- not significantly different between normal walking, quick walking and stair climbing,
- not significantly different between GD, SU, SD and BMA, but significantly higher for these four activities than for walking and stair climbing.

5. Conclusions

The main objective of this work was to evaluate the pressure fields and contact areas in the hip joint during some daily activities from numerical modelling. To do this, a parametric model based on the finite element method was developed (HJPM). The loading carried out as well as the position of the articular surfaces during the activities studied are the result of the work published by Bergmann et al. in 2001 [13]. This model makes it possible to simulate the movement and calculate the temporal evolution of pressure fields and contact areas.

Temporal pressure evolution closely mimics the applied force. In activities such as walking and stair-related motions, a bimodal pressure profile is observed, with the second peak aligning temporally with the maximal extension of the hip. Staircase descent induces higher pressure levels compared to ascent. The alternation between bipodal and monopodal stances emerges as the most physiologically restrictive activity, while the acts of sitting and rising from a chair are identified as the least restrictive. Pressure peaks exhibit varying spatial localizations across activities, predominantly concentrated in specific regions of the femoral head and cotyloid. The obtained results align with models utilizing a spherical joint paradigm.

The study covered eight activities. It would be interesting to study new activities involving high, repeated but also prolonged loads such as standing or squatting, which are a priori harmful to the articular cartilage [32,33].

To avoid the use of experimental measurements with instrumented prostheses, coupling with musculoskeletal model would offer promising clinical applications in preoperative planning, implant optimization, and joint preservation.

To reduce the model complexity and obtain a reasonable calculation time, some simplifying assumptions were necessary: a spherical shape, no inter-articular space, no friction, elastic/hyperelastic cartilage of uniform thickness, and non-deformable bones. This model can be improved in the following ways:

- by making the geometric shape more complex. As in other studies from the literature [1,3,34–36], the femoral head and cotyloid were assumed to be spherical in shape. Anderson et al. [20] showed that the spherical geometry can underestimate contact pressures by 50% and contact areas by 25% compared to a geometry more specific to a given subject. A modification of the initial spherical shape can be easily integrated in the HJPM to better understand the functioning of the pathological hip joint. In a previous study [37], the authors have demonstrated that, in pathological case, a conchoid or ellipsoid shape should be considered. Another highly versatile approach involves using the basic spherical geometry and deforming it according to a patient's morphological specifics through morphing techniques as used by Salo et al. [38]. Ghosh et al. [39] have further illustrated that incorporating an anatomical femoral head with a cartilage layer is more suitable than utilizing a perfectly spherical head. Through the application of morphing techniques, it becomes feasible to seamlessly adjust the spherical model to the anatomical model, representing a significant avenue for improvement.
- By taking into account the patient's actual geometric shape, which can be obtained from computed tomography (CT) scans [9,40], and integrating it into the parametric model allows for individualized modelling. This approach would enable us to incorporate the patient's exact joint geometry into the model, thereby reflecting the specific anatomical characteristics of each individual. Consequently, this parametrization of the model could provide precise insights on the behaviour of the

patient's hip joint. It would be particularly valuable for preoperative planning and implant optimization, ensuring a better adaptation to the unique morphology of each patient.

- by adding new constitutive structures of the coxofemoral joint. Synovial fluid has not been explicitly modelled. We assumed frictionless contact, which is justified by the low coefficients of friction measured in vivo in healthy joints [41]. It can, perhaps, play a role in the distribution of pressures within the joint [42–44], especially for non-spherical geometries. The labrum was not modelled either. It fits over the entire circumference of the cotyloid eyebrow, thus increasing the depth of the cotyloid cavity and improving the covering of the femoral head by extending the cartilaginous surface of the cotyloid. It forms a sealed circular seal around the femoral head with the transverse ligament to trap synovial fluid between the articular surfaces to reduce friction and better distribute pressures [30,43,44].
- by enriching the behaviour of cartilage. For very fast or very slow activities a visco-poro-elastic behaviour would be necessary. Another improvement is also to consider the heterogeneous properties of cartilage, experimentally identified by the authors in a previous study [22].
- by modelling the layers underlying the cartilage (subchondral bone, spongy, cortical) by deformable solids and the irregularity of the surface of the bone under chondral and the non-uniformity of the thickness of the cartilage. These assumptions may impact the results [9,20,45,46].

The hip model developed being parametric, a natural continuation of this study is the sensitivity analysis of mechanical fields to parameters (material, geometrical and load) to identify the most influential as a function of movements. This model can therefore help in the preoperative planning of peri-acetabular osteotomies of the hip, in the postoperative

rehabilitation, and illuminate new aspects of the design and positioning optimization of implants.

Acknowledgements

Funding: French Ministry of Higher Education and Research.

Competing interests: None declared.

Ethical approval: Not required

Declaration of interest

None

References

[1] Yoshida H, Faust A, Wilckens J, Kitagawa M, Fetto J, Chao EY-S. Three-dimensional dynamic hip contact area and pressure distribution during activities of daily living. J Biomech 2006;39:1996–2004. https://doi.org/10.1016/j.jbiomech.2005.06.026.

[2] Mavčič B, Pompe B, Antolič V, Daniel M, Iglič A, Kralj-Iglič V. Mathematical estimation of stress distribution in normal and dysplastic human hips. J Orthop Res 2002;20:1025–30. https://doi.org/10.1016/S0736-0266(02)00014-1.

[3] Genda E, Iwasaki N, Li G, MacWilliams BA, Barrance PJ, Chao EYS. Normal hip joint contact pressure distribution in single-leg standing—effect of gender and anatomic parameters. J Biomech 2001;34:895–905. https://doi.org/10.1016/S0021-9290(01)00041-0.

[4] Gaffney BMM, Williams ST, Todd JN, Weiss JA, Harris MD. A Musculoskeletal Model for Estimating Hip Contact Pressure During Walking. Ann Biomed Eng 2022;50:1954–63. https://doi.org/10.1007/s10439-022-03016-w.

[5] Sylvester AD, Lautzenheiser SG, Kramer PA. A review of musculoskeletal modelling of human locomotion. Interface Focus 2021;11:20200060. https://doi.org/10.1098/rsfs.2020.0060.

[6] Bachtar F, Chen X, Hisada T. Finite element contact analysis of the hip joint. Med Biol Eng Comput 2006;44:643–51. https://doi.org/10.1007/s11517-006-0074-9.

[7] Brown TD, DiGioia AM. A contact-coupled finite element analysis of the natural adult hip. J Biomech 1984;17:437–48. https://doi.org/10.1016/0021-9290(84)90035-6.

[8] Rapperport DJ, Carter DR, Schurman DJ. Contact finite element stress analysis of the hip joint. J Orthop Res 1985;3:435–46. https://doi.org/10.1002/jor.1100030406.

[9] Anderson AE, Ellis BJ, Maas SA, Peters CL, Weiss JA. Validation of Finite Element Predictions of Cartilage Contact Pressure in the Human Hip Joint. J Biomech Eng 2008;130:051008. https://doi.org/10.1115/1.2953472.

[10] Geoffrey Ng KC, Rouhi G, Lamontagne M, Beaulé PE. Finite Element Analysis Examining the Effects of Cam FAI on Hip Joint Mechanical Loading Using Subject-Specific Geometries During Standing and Maximum Squat. HSS J 2012;8:206–12. https://doi.org/10.1007/s11420-012-9292-x.

[11] Akrami M, Craig K, Dibaj M, Javadi AA, Benattayallah A. A three-dimensional finite element analysis of the human hip. J Med Eng Technol 2018;42:546–52. https://doi.org/10.1080/03091902.2019.1576795.

[12] Clarke SG, Phillips ATM, Bull AMJ. Evaluating a suitable level of model complexity for finite element analysis of the intact acetabulum. Comput Methods Biomech Biomed Engin 2013;16:717–24. https://doi.org/10.1080/10255842.2011.633906.

[13] Bergmann G, Deuretzbacher G, Heller M, Graichen F, Rohlmann A, Strauss J, et al. Hip contact forces and gait patterns from routine activities. J Biomech 2001;34:859–71. https://doi.org/10.1016/S0021-9290(01)00040-9.

[14] Modenese L, Phillips ATM. Prediction of hip contact forces and muscle activations during walking at different speeds. Multibody Syst Dyn 2012;28:157–68. https://doi.org/10.1007/s11044-011-9274-7.

[15] Wesseling M, Derikx LC, de Groote F, Bartels W, Meyer C, Verdonschot N, et al. Muscle optimization techniques impact the magnitude of calculated hip joint contact forces. J Orthop Res 2015;33:430–8. https://doi.org/10.1002/jor.22769.

[16] Henak CR, Kapron AL, Anderson AE, Ellis BJ, Maas SA, Weiss JA. Specimen-specific predictions of contact stress under physiological loading in the human hip: validation and sensitivity studies. Biomech Model Mechanobiol 2014;13:387–400. https://doi.org/10.1007/s10237-013-0504-1.

[17] Athanasiou KA, Agarwal A, Dzida FJ. Comparative study of the intrinsic mechanical properties of the human acetabular and femoral head cartilage. J Orthop Res 1994;12:340–9. https://doi.org/10.1002/jor.1100120306.

[18] Naish JH, Xanthopoulos E, Hutchinson CE, Waterton JC, Taylor CJ. MR measurement of articular cartilage thickness distribution in the hip. Osteoarthritis Cartilage 2006;14:967–73. https://doi.org/10.1016/j.joca.2006.03.017.
[19] Ateshian GA, Ellis BJ, Weiss JA. Equivalence Between Short-Time Biphasic and Incompressible Elastic Material Responses. J Biomech Eng 2007;129:405–12. https://doi.org/10.1115/1.2720918.
[20] Anderson AE, Ellis BJ, Maas SA, Weiss JA. Effects of idealized joint geometry on finite element predictions of cartilage contact stresses in the hip. J Biomech 2010;43:1351–7. https://doi.org/10.1016/j.jbiomech.2010.01.010.
[21] Pustoc'h A, Cheze L. Normal and osteoarthritic hip joint mechanical behaviour: a comparison study. Med Biol Eng Comput 2009;47:375–83. https://doi.org/10.1007/s11517-009-0457-9.
[22] Richard F, Villars M, Thibaud S. Viscoelastic modeling and quantitative experimental characterization of normal and osteoarthritic human articular cartilage using indentation. J Mech Behav Biomed Mater 2013;24:41–52. https://doi.org/10.1016/j.jmbbm.2013.04.012.
[23] Pustoc'h A. Élaboration d'un modèle mécanique de l'articulation de la hanche sous sollicitations dynamiques. Ph.D thesis, Université Claude Bernard, 2007.
[24] Pawaskar SS, Ingham E, Fisher J, Jin Z. Fluid load support and contact mechanics of hemiarthroplasty in the natural hip joint. Med Eng Phys 2011;33:96–105. https://doi.org/10.1016/j.medengphy.2010.09.009.
[25] Liu X, Zhang X, Zhong S, Jiang J. Dynamic Assessment of Contact Pressure Changes in the Hip Joint Cartilage During Daily Activities. 2018 5th Int. Conf. Syst. Inform. ICSAI, Nanjing: IEEE; 2018, p. 570–5. https://doi.org/10.1109/ICSAI.2018.8599391.
[26] Harris MD, Anderson AE, Henak CR, Ellis BJ, Peters CL, Weiss JA. Finite element prediction of cartilage contact stresses in normal human hips. J Orthop Res 2012;30:1133–9. https://doi.org/10.1002/jor.22040.
[27] McGibbon CA, Krebs DE, Trahan CA, Trippel SB, Mann RW. Cartilage degeneration in relation to repetitive pressure. J Arthroplasty 1999;14:52–8. https://doi.org/10.1016/S0883-5403(99)90202-4.
[28] Kurrat HJ, Oberlander W. The thickness of the cartilage in the hip joint. J Anat 1978;126:145–55.
[29] Adam C, Eckstein F, Milz S, Putz R. The distribution of cartilage thickness within the joints of the lower limb of elderly individuals. J Anat 1998;193:203–14. https://doi.org/10.1046/j.1469-7580.1998.19320203.x.
[30] v. Eisenhart-Rothe R, Witte H, Steinlechner M, Müller-Gerbl M, Putz R, Eckstein F. Quantitative determination of the contact pressure distribution in the hip joint during gait. Unfallchirurg 1999;102:625–31. https://doi.org/10.1007/s001130050458.
[31] Bissacotti JF, Ritter MA, Faris PM, Keating EM, Cates HE. A new radiographic evaluation of primary osteoarthritis. Orthopedics 1994;17:927–30.
[32] Lequesne M. Sport et arthrose des membres. Sci Sports 2004;19:281–5. https://doi.org/10.1016/j.scispo.2004.09.003.
[33] Magnusson ML, Pope MH. a Review of the Biomechanics and Epidemiology of Working Postures (it Isn't always Vibration which is to BLAME!). J Sound Vib 1998;215:965–76. https://doi.org/10.1006/jsvi.1998.1677.
[34] Kumagai M, Kim YH, Inoue N, Genda A, Hua K, Liong BT, et al. 3-D Dynamic Hip Contact Pressure Distribution In Daily Activities, Florida, USA: 2003, p. 53–4.
[35] Ipavec M, Brand RA, Pedersen DR, Mavčič B, Kralj-Iglič V, Iglič A. Mathematical modelling of stress in the hip during gait. J Biomech 1999;32:1229–35. https://doi.org/10.1016/S0021-9290(99)00119-0.
[36] Genda E, Konishi N, Hasegawa Y, Miura T. A computer simulation study of normal and abnormal hip joint contact pressure. Arch Orthop Trauma Surg 1995;114:202–6. https://doi.org/10.1007/BF00444263.
[37] Villars M, Fournier E, Richard F, Thibaud S. Identification of geometrical parameters of femoral heads for hip joint mechanical model. Comput Methods Biomech Biomed Engin 2011;14:247–8. https://doi.org/10.1080/10255842.2011.595215.

[38] Salo Z, Kreder H, Whyne CM. Influence of pelvic shape on strain patterns: A computational analysis using finite element mesh morphing techniques. J Biomech 2021;116:110207. https://doi.org/10.1016/j.jbiomech.2020.110207.
[39] Ghosh R, Pal B, Ghosh D, Gupta S. Finite element analysis of a hemi-pelvis: the effect of inclusion of cartilage layer on acetabular stresses and strain. Comput Methods Biomech Biomed Engin 2015;18:697–710. https://doi.org/10.1080/10255842.2013.843674.
[40] Lostado Lorza R, Somovilla Gomez F, Corral Bobadilla M, Íñiguez Macedo S, Rodríguez San Miguel A, Fernández Martínez E, et al. Comparative Analysis of Healthy and Cam-Type Femoroacetabular Impingement (FAI) Human Hip Joints Using the Finite Element Method. Appl Sci 2021;11:11101. https://doi.org/10.3390/app112311101.
[41] Jahn S, Seror J, Klein J. Lubrication of Articular Cartilage. Annu Rev Biomed Eng 2016;18:235–58. https://doi.org/10.1146/annurev-bioeng-081514-123305.
[42] Terayama K, Takei T, Nakada K. Joint Space of the Human Knee and Hip Joint under a Static Load. Eng Med 1980;9:67–74. https://doi.org/10.1243/EMED_JOUR_1980_009_017_02.
[43] Ferguson SJ, Bryant JT, Ganz R, Ito K. The influence of the acetabular labrum on hip joint cartilage consolidation: a poroelastic finite element model. J Biomech 2000;33:953–60.
[44] Ferguson SJ, Bryant JT, Ganz R, Ito K. An in vitro investigation of the acetabular labral seal in hip joint mechanics. J Biomech 2003;36:171–8. https://doi.org/10.1016/S0021-9290(02)00365-2.
[45] Kapandji AI, Merle d'Aubigné R. Physiologie articulaire. schémas commentés de mécanique humaine Fascicule III, Fascicule III,. 1975.
[46] Wei H-W, Sun S-S, Jao S-HE, Yeh C-R, Cheng C-K. The influence of mechanical properties of subchondral plate, femoral head and neck on dynamic stress distribution of the articular cartilage. Med Eng Phys 2005;27:295–304. https://doi.org/10.1016/j.medengphy.2004.12.008.